

## Relative population of states in $^{21}\text{Mg}$ from few-nucleon removal reactions

B. Longfellow<sup>1,2,3</sup>, A. Gade<sup>1,2</sup>, D. Bazin<sup>1,2</sup>, P. C. Bender<sup>1,\*</sup>, M. Bowry<sup>1,†</sup>, B. A. Brown<sup>1,2</sup>, B. Elman<sup>1,2</sup>,  
E. Lunderberg<sup>1,2</sup>, D. Rhodes<sup>1,2,‡</sup>, M. Spieker<sup>1,§</sup>, D. Weisshaar<sup>1,¶</sup> and S. J. Williams<sup>1,||</sup>

<sup>1</sup>National Superconducting Cyclotron Laboratory, Michigan State University, East Lansing, Michigan 48824, USA

<sup>2</sup>Department of Physics and Astronomy, Michigan State University, East Lansing, Michigan 48824, USA

<sup>3</sup>Lawrence Livermore National Laboratory, Livermore, California 94550, USA



(Received 24 October 2022; accepted 23 January 2023; published 30 January 2023)

Nuclear reactions with intermediate-energy beams in which three, four, and five nucleons are removed are expected to proceed through a combination of nondissipative and statistical processes. In an experiment at the National Superconducting Cyclotron Laboratory, in-beam  $\gamma$ -ray spectroscopy was utilized to study few-nucleon removal reactions from incoming beams of  $^{24}\text{Mg}$ ,  $^{25}\text{Al}$ , and  $^{26}\text{Si}$  projectiles to the same reaction product,  $^{21}\text{Mg}$ . New  $\gamma$ -ray transitions and  $\gamma$ - $\gamma$  coincidences in  $^{21}\text{Mg}$  were established using the CsI(Na) array CAESAR and the inclusive cross section for three-neutron removal from  $^{24}\text{Mg}$  was measured. Significant differences in the relative population of states in  $^{21}\text{Mg}$  from  $^{25}\text{Al}$  compared to  $^{26}\text{Si}$  were observed and found to be correlated with the spins of the  $^{21}\text{Mg}$  states. As a result, this intermediate regime between direct and statistical nucleon removal may have potential as a tool to deliver unique patterns of level populations in fast-beam experiments and alter isomer to ground state ratios in the production of exotic beams.

DOI: [10.1103/PhysRevC.107.014620](https://doi.org/10.1103/PhysRevC.107.014620)

### I. INTRODUCTION

In fast-beam experiments at rare isotope facilities, there is a fantastic opportunity to perform the in-beam  $\gamma$ -ray spectroscopy of a variety of different isotopes in the same measurement by identifying all particles in the entrance and exit channels event by event. Often, direct one-nucleon knockout reactions from intermediate-energy beams of exotic nuclei are utilized as a powerful tool in the study of single-particle nuclear structure toward the nucleon driplines [1–3]. Likewise, two-nucleon knockout has been established to proceed as a direct reaction for two-proton removal from neutron-rich nuclei [4] and two-neutron removal from neutron-deficient nuclei [5] and comparisons of the predicted and observed parallel momentum distributions have been utilized to assign spins to populated levels [6–9]. Furthermore, within the same nucleon-knockout measurements, reactions removing larger numbers of nucleons from the projectile occur at the same time, allowing further reaction products to be studied synergistically.

In the work of Obertelli *et al.*, nine reactions on intermediate-energy beams of *sd*-shell nuclei removing from two to 16 nucleons were studied [10]. The fragmentation of heavy nuclei can be modeled by the abrasion-ablation process in which the populations of excited states in the reaction products are described statistically [11]. It was observed by Obertelli *et al.* that the relative population of states in the reaction products could be described through a purely statistical process when six or more nucleons were removed. However, for the three- and four-nucleon removal reactions considered, a combination of direct and statistical mechanisms was required to best describe the data [10]. In this work, we explore three-, four-, and five-nucleon removal reactions belonging to this transition region where nondissipative and statistical processes compete:  $^9\text{Be}(^{24}\text{Mg}, ^{21}\text{Mg} + \gamma)X$ ,  $^9\text{Be}(^{25}\text{Al}, ^{21}\text{Mg} + \gamma)X$ , and  $^9\text{Be}(^{26}\text{Si}, ^{21}\text{Mg} + \gamma)X$ .

The neutron-deficient nucleus  $^{21}\text{Mg}$  ( $Z = 12$ ,  $N = 9$ ) lies close to the proton dripline being the second-lightest Mg isotope with its ground state bound to the emission of protons. Excited states in  $^{21}\text{Mg}$  have been probed via the three neutron transfer reaction  $^{24}\text{Mg}(^3\text{He}, ^6\text{He})^{21}\text{Mg}$  [12,13],  $^{20}\text{Na} + p$  resonant elastic scattering [14], the one-neutron knockout reaction  $^9\text{Be}(^{22}\text{Mg}, ^{21}\text{Mg} + \gamma)X$  [15], and low-energy Coulomb excitation [16]. Furthermore, levels in  $^{21}\text{Mg}$  near the proton separation energy of 3326(16) keV [17] have received particular attention due to their role in calculations of the  $^{20}\text{Na}(p, \gamma)^{21}\text{Mg}$  reaction rate [13], which was investigated as part of a possible breakout path from the hot CNO cycle to the *rp* process but is now suggested to not play a significant role in explosive hydrogen burning in astrophysical sites [14].

In the present work, few-nucleon removal reactions were leveraged to place new  $\gamma$ -ray transitions in the  $^{21}\text{Mg}$  level

\*Present address: Department of Physics, University of Massachusetts Lowell, Lowell, Massachusetts 01854, USA.

†Present address: University of the West of Scotland, Paisley PA1 2BE, UK.

‡Present address: TRIUMF, 4004 Wesbrook Mall, Vancouver, BC V6T 2A3, Canada.

§Present address: Department of Physics, Florida State University, Tallahassee, Florida 32306, USA.

¶Present address: Diamond Light Source, Harwell Science and Innovation Campus, Didcot, Oxfordshire OX110DE, UK.

scheme and tentatively assign spins and parities in conjunction with comparisons with the mirror nucleus and shell-model calculations. In addition, the first inclusive cross section measurement for three-neutron removal from  $^{24}\text{Mg}$  is reported. A large difference in the population of the  $1/2^-$  level in  $^{21}\text{Mg}$  was observed between few-nucleon removal from  $^{25}\text{Al}$  and  $^{26}\text{Si}$ . This unexpected result was further probed revealing large asymmetries in the relative populations of levels in  $^{21}\text{Mg}$  produced from  $^{25}\text{Al}$  and  $^{26}\text{Si}$  that are correlated with the populated states' spins. Consequently, the few-nucleon removal reaction may have the potential to yield unique population patterns compared to selective knockout and statistical fragmentation making it a useful mechanism for spectroscopy. Furthermore, it may be able to be exploited to offer some degree of control in the ratio of isomer to ground state population in rare isotope beam production.

## II. EXPERIMENT

The measurements were performed using the Coupled Cyclotron Facility at the National Superconducting Cyclotron Laboratory [18]. A cocktail secondary beam was produced by fragmenting the 150 MeV/u  $^{36}\text{Ar}$  primary beam on a 550 mg/cm $^2$   $^9\text{Be}$  target at the midacceptance position of the A1900 fragment separator [19]. The secondary beam was purified using a 250 mg/cm $^2$  achromatic Al wedge leading to a composition of 54.5%  $^{24}\text{Mg}$ , 29.5%  $^{25}\text{Al}$ , and 13.5%  $^{26}\text{Si}$ . The species constituting the secondary beam were unambiguously identified via time of flight between a plastic scintillator at the exit of the A1900 and a plastic scintillator at the object position of the analysis beamline of the S800 magnetic spectrograph [20]. A 287(3) mg/cm $^2$   $^9\text{Be}$  target was placed at the reaction target position of the S800 and the midtarget energies for the incoming  $^{24}\text{Mg}$ ,  $^{25}\text{Al}$ , and  $^{26}\text{Si}$  beams were 95, 102, and 109 MeV/u, respectively. Outgoing reaction products were identified on an event-by-event basis using the standard set of S800 focal plane detectors [21]. The particle identification plot utilizing the energy loss in the S800 ionization chamber and time-of-flight from the plastic scintillators in the beamline to the plastic scintillator at the back of the S800 focal plane for reaction products from the  $^{26}\text{Si}$  incoming beam is shown in Refs. [22,23]. The parallel momentum of each reaction product was determined from the trajectory of the projectile from the reaction target to the S800 focal plane reconstructed using position and angle information from the two  $xy$ -position sensitive cathode-readout drift chambers (CRDCs) and the magnetic rigidity setting of the S800 spectrograph. In this experiment, the S800 analysis beamline was operated in dispersion-matched mode to optimize momentum resolution.

The original goal of the experiment was to benchmark the sensitivity of the widths and shapes of parallel momentum distributions following direct two-neutron knockout to the details of the initial- and final-state wave functions as predicted by shell-model calculations in conjunction with eikonal reaction theory [24]. The results of this study for the two-neutron knockout products  $^{22}\text{Mg}$ ,  $^{23}\text{Al}$ , and  $^{24}\text{Si}$  were recently published and are available in Ref. [9]. The focus of the present work is on complementary few-nucleon removal

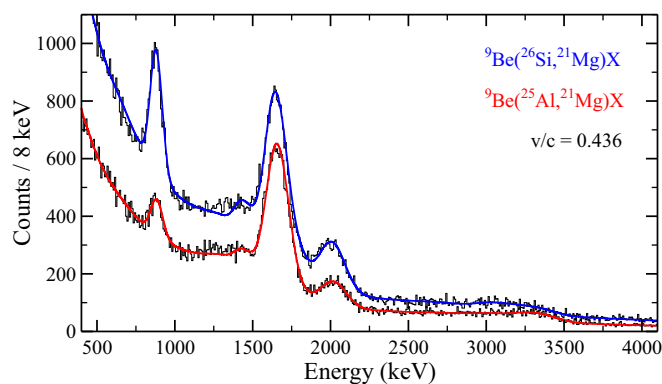


FIG. 1. Doppler-corrected  $\gamma$ -ray spectra for the five- and four-nucleon removal reactions  $^9\text{Be}(^{26}\text{Si}, ^{21}\text{Mg} + \gamma)\text{X}$  and  $^9\text{Be}(^{25}\text{Al}, ^{21}\text{Mg} + \gamma)\text{X}$ . The solid blue and red curves are GEANT4 simulations of the observed transitions (see text) with a double exponential background model fit to the data from the incoming  $^{26}\text{Si}$  and  $^{25}\text{Al}$  beams, respectively.

reactions from the same secondary beams resulting in  $^{21}\text{Mg}$  projectiles.

To identify excited states in the  $^{21}\text{Mg}$  reaction residues by their de-excitation  $\gamma$  rays, the 287(3) mg/cm $^2$   $^9\text{Be}$  reaction target was surrounded by the CAESium-iodide scintillator ARray (CAESAR) [25]. The high granularity and efficiency of this 192-element array of CsI(Na) scintillators enabled Doppler reconstruction of the  $\gamma$  rays emitted by the  $^{21}\text{Mg}$  projectiles in flight. The in-beam response of CAESAR after Doppler reconstruction was modeled using GEANT4 simulations benchmarked against laboratory-frame  $\gamma$ -ray energy spectra from standard  $\gamma$ -ray calibration sources. A systematic uncertainty in Doppler-corrected energy of 4.5 keV was adopted based on measurements of known  $\gamma$ -ray transitions in  $^{22}\text{Mg}$  and  $^{23}\text{Mg}$  as discussed in Ref. [22]. The energy-dependent efficiency curve from the GEANT4 simulation was scaled to match the efficiency curve derived from the source measurements following the method of Ref. [26] resulting in an efficiency uncertainty of 5%.

## III. RESULTS

### A. Four- and five-nucleon removal

The Doppler-corrected  $\gamma$ -ray spectra for  $^{21}\text{Mg}$  reaction residues produced from the  $^{25}\text{Al}$  and  $^{26}\text{Si}$  incoming projectiles are shown in Fig. 1. For all  $\gamma$ -ray spectra, nearest-neighbor adback was utilized. Furthermore, the  $v/c$  in Fig. 1 corresponds to the central trajectory through the S800 spectrograph. The magnetic rigidity of the spectrograph was set to 2.55250 Tm. The trajectory reconstructed event by event from the S800 focal plane detectors was accounted for in the Doppler correction. A striking difference can be clearly seen in the relative population of the excited states in the two reaction channels, in particular for the 883.3(8) keV [15] transition from the  $1/2^-$  level to the  $1/2^+$  first excited state of  $^{21}\text{Mg}$  at 205.6(1) keV, which is isomeric with an 11.7(5) ns half-life [16] and therefore could not be observed in the present in-flight experiment.

The region around 1660 keV is a multiplet due to the known 1651(4) keV [15] and 1672(1) keV [16] transitions. However, the  $3/2^+$  1651(4) keV level has 1451(4) keV and 1651(4) keV  $\gamma$ -decay branches to the isomer and ground state with relative intensities of 22(9)% and 100(9)% [15], respectively, while the  $9/2^+$  1672(1) keV level only  $\gamma$  decays to the  $5/2^+$  ground state [16]. To better constrain this region, the intensity ratio of the 1451 keV and 1651 keV transitions was fixed to the literature value in the fits. Similarly, the 2000 keV region contains the known 1989(3) keV transition [15]. However, there is a level at 2048(15) keV observed in three-neutron transfer [13] and the mirror level in  $^{21}\text{F}$ , assigned ( $5/2^-$ ), was only observed to  $\gamma$  decay to the ground state [27]. The  $3/2^-$  1989(3) keV level  $\gamma$  decays to both the isomer and ground state with relative intensities of 67(13)% and 100(13)% [15], respectively, allowing the fit region to be better constrained by fixing the known branching ratio for the 1989 keV level in the fit and including the 2048 keV transition, which we assign ( $5/2^-$ ) based on mirror comparisons.

The three-neutron transfer study also established levels in  $^{21}\text{Mg}$  at 3086(15) keV, 3244(15) keV, 3347(15) keV, and 3643(15) keV with tentative spins of ( $3/2^+$ ,  $5/2^+$ ) for the lower two states and ( $7/2^+$ ,  $9/2^+$ ) for the higher two states [13]. Note that in Ref. [13] the 3347(15) keV level was originally tentatively assigned  $7/2^+$  based on the observed angular momentum transfer of  $\ell = 4$  and comparison with states in  $^{21}\text{F}$  populated via  $\beta$  decay [28]. However, as noted in Ref. [28], the observed  $\gamma$  decay branching also matches well with shell-model calculations for the second  $9/2^+$  state. Consequently, we adopt the more conservative ( $7/2^+$ ,  $9/2^+$ ) assignment for the mirror level from Ref. [27]. Calculations using the USDB interaction [29] predict four levels between about 3.5 to 3.6 MeV with spins of  $5/2_2^+$ ,  $9/2_2^+$ ,  $3/2_2^+$ , and  $7/2_1^+$  in  $^{21}\text{Mg}$ .

In the shell-model calculation, the  $5/2_2^+$  and  $3/2_2^+$  states are predicted to have  $\gamma$  decay branches to the  $3/2_1^+$  level at 1651 keV experimentally while the  $9/2_2^+$  and  $7/2_1^+$  states are predicted to have  $\gamma$  decay branches to the  $9/2_1^+$  level at 1672 keV experimentally. The experimental data on the  $\gamma$ -ray transitions in the mirror nucleus  $^{21}\text{F}$  is consistent with these predictions [27]. Therefore, considering the known 3086 keV, 3244 keV, 3347 keV, and 3643 keV levels in  $^{21}\text{Mg}$ , possible coincidences in the present work are 1651–1435 keV, 1651–1593 keV, 1672–1675 keV, and 1672–1971 keV (along with coincidences with the less intense 1451 keV branch from the 1651 keV level). To determine the possible presence of these transitions for the first time, the multiplicity two  $\gamma$ - $\gamma$  coincidences measured with CAESAR were gated on the 1660 keV region from 1300 to 2200 keV to include the full-energy peaks of the possible 1435 keV and 1971 keV transitions and then background subtracted using a gate of equal width at energies above this region for both  $^{21}\text{Mg}$  produced from  $^{25}\text{Al}$  and  $^{26}\text{Si}$ . The resulting spectra are shown in Fig. 2. The self-coincident peak was fit with possible  $\gamma$ - $\gamma$  coincidence spectra from the known 3–3.7 MeV levels and is well described by a combination of a 1593 keV  $\gamma$  ray from the 3244 keV level to the 1651 keV state (the known branching ratios from the 1651 keV level were also accounted for and fixed in the fit) and a 1675 keV  $\gamma$  ray from the 3347 keV state

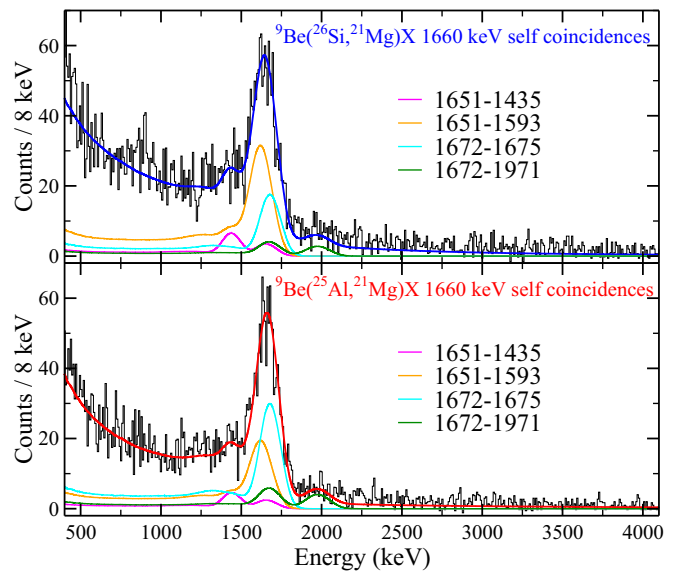


FIG. 2. Background-subtracted multiplicity two  $\gamma$ - $\gamma$  coincidences gated on the 1660 keV region for  $^{21}\text{Mg}$  produced from the incoming  $^{26}\text{Si}$  (top) and  $^{25}\text{Al}$  (bottom) beams. The strongly self-coincident peak was fit with predicted coincidences from known levels, see text for details.

to the 1672 keV level. The possible 1435 keV  $\gamma$ -ray transition from the 3086 keV level to the 1651 keV state and 1971 keV  $\gamma$ -ray transition from the 3643 keV level to the 1672 keV state were not clearly observed and could be omitted without affecting the fit quality.

For direct transitions to the ground state or isomer, only one  $\gamma$  ray is emitted in the vicinity of CAESAR. Therefore, a relative enhancement in the multiplicity one spectrum of Fig. 3 compared to the singles spectrum of Fig. 1 is observed

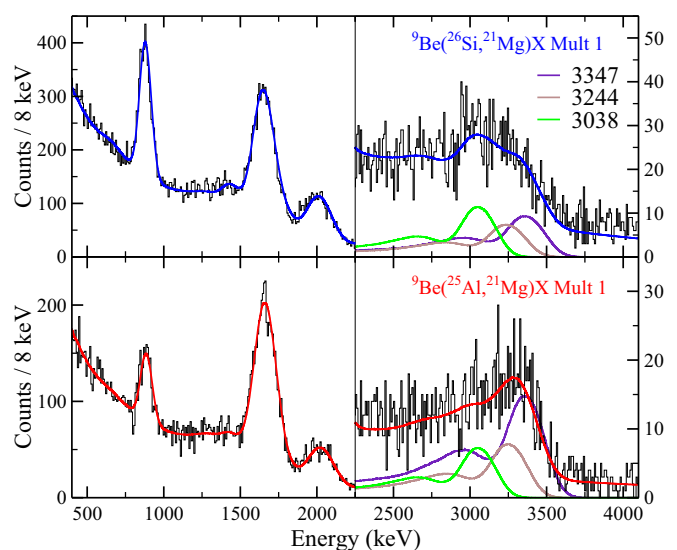


FIG. 3. Doppler-corrected  $\gamma$ -ray spectra for  $^{21}\text{Mg}$  produced from  $^{26}\text{Si}$  (top) and  $^{25}\text{Al}$  (bottom) secondary beams gated on multiplicity one events. The high energy range highlights the difference in  $\gamma$ -ray transition intensities around 3–3.5 MeV.

TABLE I. Efficiency-corrected relative intensities for transitions in  $^{21}\text{Mg}$  produced via few-nucleon knockout from  $^{26}\text{Si}$  and  $^{25}\text{Al}$  projectiles. Intensities are reported relative to the 1651 keV transition for both data sets.

Energy (keV)	$J_i^\pi \rightarrow J_f^\pi$	$^{26}\text{Si}$	$^{25}\text{Al}$
883	$1/2_1^- \rightarrow 1/2_1^+$	56(3)	31(3)
1451	$3/2_1^+ \rightarrow 1/2_1^+$	22(14) <sup>a</sup>	22(17) <sup>a</sup>
1593	$(3/2_2^+, 5/2_2^+) \rightarrow 3/2_1^+$	29(13)	32(16)
1651	$3/2_1^+ \rightarrow 5/2_1^+$	100(14) <sup>a</sup>	100(17) <sup>a</sup>
1672	$9/2_1^+ \rightarrow 5/2_1^+$	37(16)	118(40)
1675	$(7/2_1^+, 9/2_2^+) \rightarrow 9/2_1^+$	14(7)	43(23)
1783	$3/2_1^- \rightarrow 1/2_1^+$	25(7) <sup>b</sup>	15(9) <sup>b</sup>
1989	$3/2_1^- \rightarrow 5/2_1^+$	38(7) <sup>b</sup>	22(9) <sup>b</sup>
2048	$(5/2_1^-) \rightarrow 5/2_1^+$	26(5)	34(8)
3038	$(3/2_2^+, 5/2_2^+) \rightarrow 1/2_1^+$	10(5)	12(7)
3244	$(3/2_2^+, 5/2_2^+) \rightarrow 5/2_1^+$	7(4)	13(7)
3347	$(7/2_1^+, 9/2_2^+) \rightarrow 5/2_1^+$	10(5)	25(11)

<sup>a</sup> $3/2_1^+$  branching ratio [15] fixed in fits.

<sup>b</sup> $3/2_1^-$  branching ratio [15] fixed in fits.

for the peaks corresponding to these transitions. As was the case in the coincidence data, the 3643 keV state is not clearly visible in Fig. 3. In the shell-model calculations using the USDB Hamiltonian the  $5/2_2^+$  state has a significant  $\gamma$  decay branch to the ground state while the branch to the isomer has a relative intensity of 3% (the branch to the  $3/2_1^+$  level is 72%). On the other hand, the  $3/2_2^+$  level decays to the ground state, isomer, and  $3/2_1^+$  level with relative intensities of 51%, 100%, and 94%, respectively. For the  $7/2_1^+$  level, the relative intensities are 60% to the ground state and 100% to the  $9/2_1^+$  state while for the  $9/2_2^+$  level, the relative intensities are 20% to the ground state and 100% to the  $9/2_1^+$  level. As discussed above, the  $(3/2_2^+, 5/2_2^+)$  3244 keV state may  $\gamma$  decay to both the ground state and isomeric state and transitions at 3244 keV and 3038 keV were included in the fits. The high energy range of Fig. 3 shows that the  $(7/2_1^+, 9/2_2^+)$  3347 keV state is more strongly populated in few-nucleon removal from  $^{25}\text{Al}$  than  $^{26}\text{Si}$  and vice versa for the  $(3/2_2^+, 5/2_2^+)$  3244 keV state. This is consistent with the  $\gamma - \gamma$  coincidences in Fig. 2. Note that the 3038 keV and 3244 keV transitions from the 3244 keV level should have the same relative intensities for both  $^{21}\text{Mg}$  produced from  $^{26}\text{Si}$  and  $^{25}\text{Al}$ . The relative intensity difference in Fig. 3 is within uncertainties but could also be explained from a small contribution of a 3086 keV peak that is stronger in the  $^{26}\text{Si}$  data set than the  $^{25}\text{Al}$  data set. The possible 1435 keV branch from the 3086 keV level, predicted to be comparable to the branch to the ground state in the shell-model calculations, was not unambiguously observed in the  $\gamma - \gamma$  coincidence data of Fig. 2.

Table I shows the extracted efficiency-corrected relative intensities for  $\gamma$ -ray transitions in  $^{21}\text{Mg}$  from fits using GEANT4 simulations of the observed peaks with a double exponential background to the data of Fig. 1. The previously measured branching ratios for the  $3/2_1^+$  and  $3/2_1^-$  levels [15] were fixed in the fits. Furthermore, the relative intensities of the 1593 keV

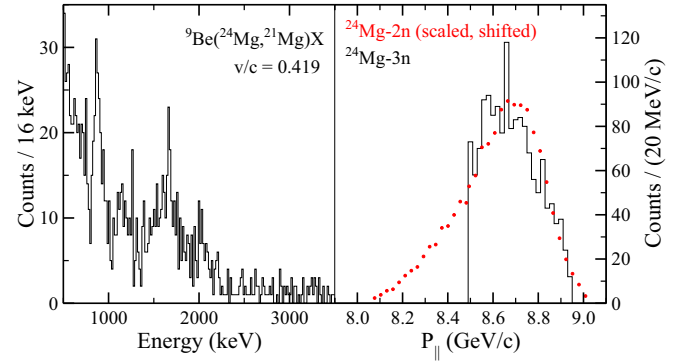


FIG. 4. Left: Doppler-corrected  $\gamma$ -ray spectra for the three-neutron removal reaction  $^9\text{Be}(^{24}\text{Mg}, ^{21}\text{Mg})X$ . Right: parallel momentum ( $P_{\parallel}$ ) distribution for  $^{21}\text{Mg}$  residues (black) reconstructed using the S800 focal plane detectors. The magnetic rigidity of the S800 for the  $^{24}\text{Mg} - 3n$  setting was 2.41881 Tm. The parallel momentum distribution for  $^{22}\text{Mg}$  residues from the same incoming  $^{24}\text{Mg}$  beam (red) with momentum shifted and counts scaled was used to roughly estimate the acceptance loss for  $^{21}\text{Mg}$ .

and 1675 keV transitions were constrained from the coincidence data of Fig. 2.

In summary, the new nuclear data results from this work are the spin-parity assignment of the 2048-keV level as  $(5/2^-)$  from mirror comparisons, the identification of strong  $\gamma - \gamma$  coincidences in the 1660 keV multiplet region, and the first observation of  $\gamma$  decay from states above 3 MeV identified previously through particle transfer at 3244 keV and 3347 keV.

## B. Three-neutron removal

Three-neutron removal from a neutron-deficient nucleus may be dominated by direct, nondissipative processes since statistical neutron emission is hindered by the large differences in proton and neutron separation energies. The Doppler-corrected  $\gamma$ -ray spectrum for  $^{21}\text{Mg}$  nuclei produced from three-neutron removal from  $^{24}\text{Mg}$  is shown in the left panel of Fig. 4. Here, a lower rigidity of the S800 spectrograph at 2.41881 Tm was utilized. The 883-keV transition from the  $1/2_1^-$  level to the isomer is clearly visible along with features around 1660 keV and 2000 keV. The statistics in this case are not sufficient to determine if the 1660 keV region is in self-coincidence as it was for  $^{21}\text{Mg}$  produced from  $^{25}\text{Al}$  and  $^{26}\text{Si}$ . For three-neutron removal, the 883-keV peak intensity relative to the 1660 keV multiplet intensity is larger compared to both four-nucleon removal from  $^{25}\text{Al}$  and five-nucleon removal from  $^{26}\text{Si}$ . For one-neutron knockout, neglecting the ground state and isomer, the largest cross section was to the  $1/2_1^-$  state and was about 2.5 times the cross section to the  $3/2_1^+$  level [15].

The right panel of Fig. 4 shows the parallel momentum distribution of the  $^{21}\text{Mg}$  reaction products reconstructed using the focal plane detectors of the S800 spectrograph and the known S800 magnetic rigidity setting. The parallel momentum distribution filled the S800 focal plane and was cut off on the low momentum side. The loss due to the acceptance of the

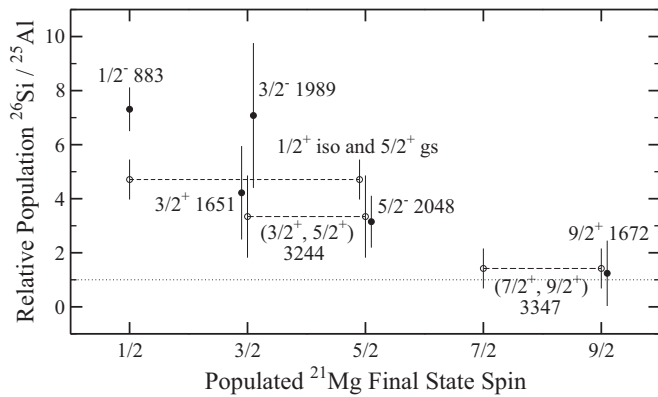


FIG. 5. Correlation between the ratio of the population of levels in  $^{21}\text{Mg}$  produced from  $^{26}\text{Si}$  to the population of levels in  $^{21}\text{Mg}$  produced from  $^{25}\text{Al}$  with the spin of the populated  $^{21}\text{Mg}$  state. Some of the spins are slightly offset for readability. The closed circles represent states with assigned spins and parities while the open circles connected with dashed lines represent states with two possible spin values along with the combined ground state and isomer which could not be distinguished in the present experimental scheme. The dotted line is a ratio of one.

S800 was estimated from the shape of the inclusive  $^{24}\text{Mg}$   $-2n$  momentum distribution measured in the present experiment and accounted for with an assumption of 100% uncertainty on the number of lost counts since the shapes of the distributions, including the low-momentum tails, should not be identical. The  $^{22}\text{Mg}$  distribution was generated from multiple S800 magnetic rigidity settings [9], which only probed the extreme high momentum side for  $^{21}\text{Mg}$ , and was shifted in momentum and scaled to match the  $^{21}\text{Mg}$  distribution. For comparison, the widths of the inclusive parallel momentum distributions for  $^{22}\text{Mg}$   $-1n$  [15] and  $^{22}\text{Mg}$   $-2n$  [7] were similar. However, the present three-neutron removal distribution may be wider than the two-neutron knockout distribution, making the estimate a lower limit. Including the effect of acceptance loss, the inclusive cross section for three-neutron removal from  $^{24}\text{Mg}$  was measured to be 0.14(6) mb. The measured inclusive three-neutron removal cross section is roughly 15 times smaller than the inclusive two-neutron knockout cross section from  $^{24}\text{Mg}$  [9] providing a benchmark for theory efforts to model three-nucleon removal in cases like this where the removal may be direct.

#### IV. DISCUSSION

The relative population of the states in  $^{21}\text{Mg}$  from few-nucleon removal from the  $^{25}\text{Al}$  and  $^{26}\text{Si}$  incoming beams is plotted in Fig. 5. To calculate the population of the states, the measured efficiency-corrected  $\gamma$ -ray intensities were utilized and the contributions from  $\gamma$ -ray transitions directly feeding the levels was accounted for. The isomer and ground states were treated together since the isomer could not be observed in the present experimental setup. The relative number of incoming  $^{26}\text{Si}$  and  $^{25}\text{Al}$  particles was accounted for in the ratio but no corrections for S800 acceptance cuts on the respective parallel momentum distributions were performed. As can be

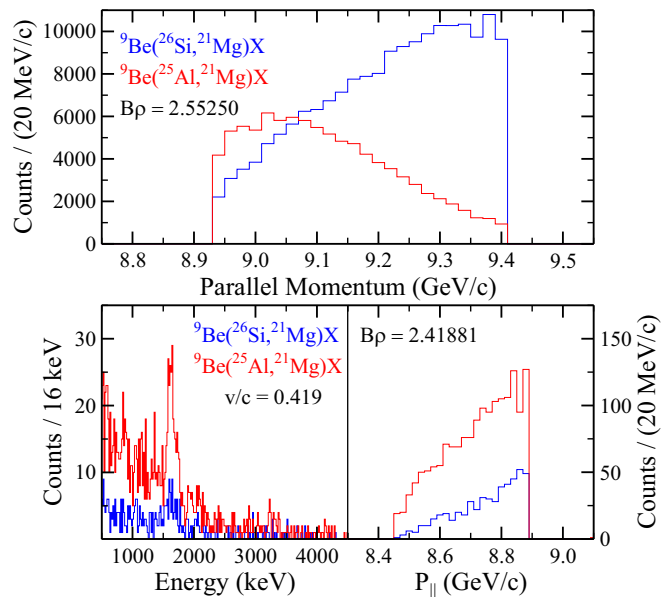


FIG. 6. Top: inclusive parallel momentum distributions for  $^{21}\text{Mg}$  reaction products from incoming  $^{26}\text{Si}$  (blue) and  $^{25}\text{Al}$  (red). The magnetic rigidity ( $B\rho$ ) of the S800 in this setting was 2.55250 Tm. The setting samples the lower momentum region for  $^{21}\text{Mg}$  from  $^{26}\text{Si}$  and the higher momentum region for  $^{21}\text{Mg}$  from  $^{25}\text{Al}$ . Bottom: the left panel shows the Doppler-corrected  $\gamma$ -ray spectra for  $^{21}\text{Mg}$  from  $^{26}\text{Si}$  and  $^{25}\text{Al}$  for the 2.41881 Tm setting. As shown in the right panel, this setting probes only the low momentum tails.

seen in Fig. 5, there is a correlation between the population of states in  $^{21}\text{Mg}$  from  $^{26}\text{Si}$  relative to the population of states in  $^{21}\text{Mg}$  from  $^{25}\text{Al}$  and the spin of the populated  $^{21}\text{Mg}$  level.

One difference in the experimental conditions for the  $^{21}\text{Mg}$  data sets from  $^{25}\text{Al}$  and  $^{26}\text{Si}$  is the portion of the inclusive parallel momentum distribution within the acceptance of the S800 magnetic spectrograph for the 2.55250 Tm setting discussed in the Results. As seen in the top panel of Fig. 6, the higher momentum portion of the parallel momentum distribution is within the S800 acceptance for  $^{21}\text{Mg}$  from  $^{25}\text{Al}$  while the lower momentum portion of the parallel momentum distribution is within the S800 acceptance for  $^{21}\text{Mg}$  from  $^{26}\text{Si}$ . The widths of exclusive parallel momentum distributions depend on the angular momentum of the removed nucleon in one-nucleon knockout or on the total angular momentum of the removed nucleons in two-nucleon knockout. Therefore, the reaction dynamics in few-nucleon removal may yield exclusive momentum distributions with differing widths. For the lower S800 magnetic rigidity setting of 2.41881 Tm shown in the bottom panel of Fig. 6, it can be seen that the 883 keV transition from the  $1/2^-$  level is no longer visible for  $^{21}\text{Mg}$  from  $^{26}\text{Si}$  in the extreme low momentum tail of the distribution. However, this does not explain the discrepancy in  $1/2^-$  population between  $^{21}\text{Mg}$  produced from  $^{25}\text{Al}$  and  $^{26}\text{Si}$  in Fig. 5 since the 883 keV peak is already more prominent in the  $^{26}\text{Si}$  data in the 2.55250 Tm setting.

In previous two-nucleon knockout measurements, relative shifts in the exclusive parallel momentum distributions of states in the same nucleus were observed [8,9]. In both cases,

the momentum distribution for knockout from the  $0^+$  ground state of an even-even nucleus to a  $4^+$  state was shifted to slightly lower momentum than for knockout to  $0^+$  and  $2^+$  levels. However, in the present work, the higher spin levels in  $^{21}\text{Mg}$  are more strongly populated from  $^{25}\text{Al}$  than  $^{26}\text{Si}$ . Since the  $^{25}\text{Al}$  data samples a higher-momentum portion of the distribution than the  $^{26}\text{Si}$  data in the 2.55250 Tm setting, any similar shifts would have to be in the opposite direction to explain the correlation observed in Fig. 5.

A possible explanation for the observed difference in the relative population of states as a function of spin is that part of the few-nucleon removal cross section may be due to the removal of particle clusters. For example, starting with  $^{26}\text{Si}$ ,  $L = 0$   $\alpha$  particle removal would mainly go to the  $^{22}\text{Mg}$   $0^+$  ground state. On the other hand, since only one proton and three neutrons are removed from the higher-spin  $^{25}\text{Al}$  ground state, the  $\alpha$  channel is closed. Starting with the  $^{25}\text{Al}$   $5/2^+$  ground state,  $L = 0$   $^3\text{He}$  ( $J = 1/2$ ) removal would mainly go to the  $^{22}\text{Mg}$   $4^+$  state. Other  $L$  values would lead to a wider range of  $J$  values in  $^{22}\text{Mg}$ . Neutron knockout from the  $^{22}\text{Mg}$   $0^+$  ground state strongly populates lower-spin, single-hole  $p$  shell and  $sd$  shell states [15]. Conversely, for example,  $p_{1/2}$  neutron removal from the  $J = 2$  and 4 states in  $^{22}\text{Mg}$  could not populate the  $1/2^-$  level in  $^{21}\text{Mg}$ . It is difficult to make quantitative calculations of these cluster removal cross sections.

To explore this possibility qualitatively, data on  $^{22}\text{Mg}$  reaction products from  $^{26}\text{Si}$  and  $^{25}\text{Al}$  incoming beams taken in the  $^{28}\text{S}$ - $1n$  setting of the in-beam  $\gamma$ -ray spectroscopy experiment described in Ref. [30] were utilized. This experiment was also the source of the  $^{22}\text{Mg}$ - $1n$  results [15] in a different setting. The experimental scheme in this case was the same as in the present work except the segmented high purity germanium array SeGA [31] was used for  $\gamma$ -ray detection rather than CAESAR. In the  $^{28}\text{S}$ - $1n$  setting, the  $N = 12$  isotones  $^{25}\text{Al}$  and  $^{26}\text{Si}$  were also constituents of the cocktail secondary beam. The incoming beam energies at the middle of the 188(4) mg/cm<sup>2</sup>  $^9\text{Be}$  target in front of the S800 spectrograph were 67 MeV/u for  $^{25}\text{Al}$  and 72 MeV/u for  $^{26}\text{Si}$ .

The top and middle panels of Fig. 7 show the Doppler-corrected  $\gamma$ -ray spectra for  $^{22}\text{Mg}$  produced from  $^{25}\text{Al}$  and  $^{26}\text{Si}$ . The insets show that the sampling of the parallel momentum distributions for  $^{22}\text{Mg}$  is similar to the sampling for  $^{21}\text{Mg}$  in Fig. 6. With the given statistics, only the 1247 keV  $2_1^+ \rightarrow 0_1^+$  and 2061 keV  $4_1^+ \rightarrow 2_1^+$  transitions are clearly visible. An analogous plot to Fig. 5 is shown in the bottom panel of Fig. 7. As before, the relative number of incoming  $^{26}\text{Si}$  and  $^{25}\text{Al}$  particles was accounted for in the ratio of efficiency-corrected intensities but no corrections for the S800 acceptance were made. As anticipated from the cluster removal argument, the  $^{22}\text{Mg}$   $0^+$  ground state is more strongly populated from incoming  $^{26}\text{Si}$  than from  $^{25}\text{Al}$ . Similar to  $^{21}\text{Mg}$ , there is a correlation between the observed relative intensities of  $^{22}\text{Mg}$  levels populated from few-nucleon removal from  $^{26}\text{Si}/^{25}\text{Al}$  with the spin of the populated  $^{22}\text{Mg}$  state, although the slope is not as extreme as in the  $^{21}\text{Mg}$  case. Consequently, part of the observed correlation for  $^{21}\text{Mg}$  could be explained by clustering. Since the parallel momentum distribution sampling

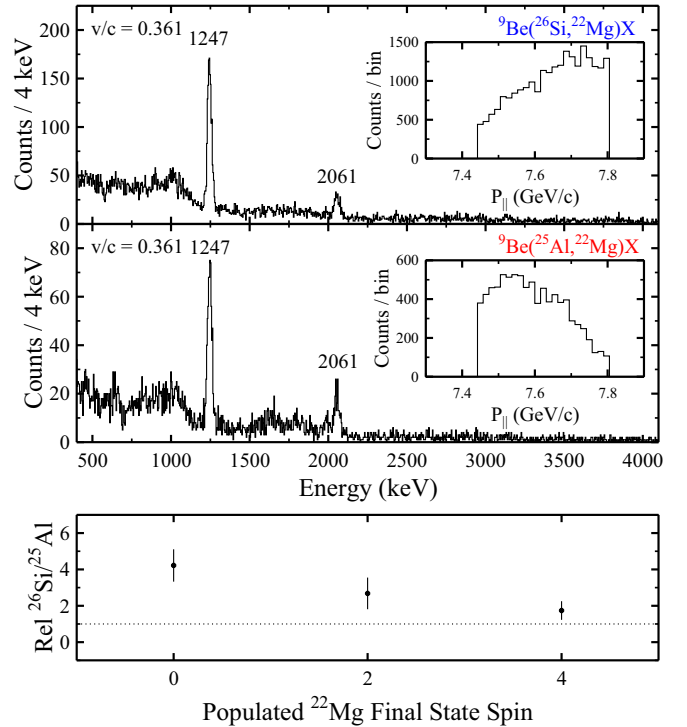


FIG. 7. Doppler-corrected  $\gamma$ -ray spectra measured by SeGA for  $^{22}\text{Mg}$  produced from  $^{26}\text{Si}$  (top) and  $^{25}\text{Al}$  (middle) secondary beams. The insets show the portions of the parallel momentum distributions sampled due to the acceptance cutoff of the S800. The magnetic rigidity setting was 2.12350 Tm. Bottom: ratio of the population of levels in  $^{22}\text{Mg}$  produced from  $^{26}\text{Si}$  to the population of levels in  $^{22}\text{Mg}$  produced from  $^{25}\text{Al}$  as a function of the spin of the populated  $^{22}\text{Mg}$  state. The dotted line is a ratio of one.

was similar for  $^{21}\text{Mg}$  and  $^{22}\text{Mg}$ , the acceptance cuts, it is possible that they also play a role in the correlation. We have shown that the angular momentum selection rules associated with cluster transfer can qualitatively explain the data. This suggests that some aspect of cluster transfer is involved but detailed calculations for cluster knockout are beyond the scope of this project.

The present results for the relative  $\gamma$ -ray intensities for  $^{21}\text{Mg}$  could be improved upon through measurements with an array of high-resolution  $\gamma$ -ray detectors, particularly for the multiplet regions around 1660 keV and 2000 keV. Furthermore, it would be interesting to determine if similar correlations between relative population of levels and the spin of the level are present for other few-nucleon removal reactions. This phenomenon could be exploited, for example, to target the population of lower or higher spin levels or to more selectively control the relative populations of ground state and isomer components in intermediate-energy secondary beams, see, e.g., [32–35]. With new, high-acceptance experimental equipment like the planned High Rigidity Spectrometer at the Facility for Rare Isotope Beams, it is anticipated to be possible to perform similar few-nucleon removal measurements at the same time as one- or two-nucleon knockout experiments that sample the parallel momentum distributions more fully.

## V. SUMMARY

Few-nucleon removal reactions were utilized to populate levels in the neutron-deficient nucleus  $^{21}\text{Mg}$  in an in-beam  $\gamma$ -ray spectroscopy experiment at the National Superconducting Cyclotron Laboratory using CAESAR for  $\gamma$ -ray detection and the S800 magnetic spectrograph for particle identification. New  $\gamma$ -ray transitions and  $\gamma$ - $\gamma$  coincidences in  $^{21}\text{Mg}$ , anticipated from known levels, were measured for the first time. The cross section for three-neutron removal from incoming  $^{24}\text{Mg}$  projectiles was measured to be 0.14(6) mb. For  $^{21}\text{Mg}$  residues produced from  $^{25}\text{Al}$  and  $^{26}\text{Si}$  incoming beams, an unexpected, strong correlation between the relative population of the states in  $^{21}\text{Mg}$  and the spin of the populated level was observed. Several hypotheses for the origin of the correlation were explored including differences in the portions of the parallel momentum distributions within the S800 momentum acceptance window and differences in the available particle removal channels from  $^{25}\text{Al}$  and  $^{26}\text{Si}$ . Ultimately, more experimental and theoretical efforts will be necessary to better understand the interplay between

statistical and nondissipative contributions in the complex region between knockout and fragmentation. However, regardless of the origin of the observed effect, the few-nucleon removal reaction shows promise as a tool to deliver unique patterns of state populations for use in both beam delivery and experimentation.

## ACKNOWLEDGMENTS

This work was supported by the National Science Foundation (NSF) under Grants No. PHY-1102511 and PHY-1565546, by the DOE National Nuclear Security Administration through the Nuclear Science and Security Consortium, under Grant No. DE-NA0003180, and by the Department of Energy, Office of Nuclear Physics, under Grant No. DE-SC0020451. Work at LLNL was performed under DOE Contract No. DE-AC52-07NA27344 and was supported by the LLNL-LDRD Program under Project No. 23-LW-047. B.A.B. acknowledges support from NSF Grant No. PHY-1811855.

- 
- [1] P. G. Hansen and J. A. Tostevin, *Annu. Rev. Nucl. Part. Sci.* **53**, 219 (2003).
- [2] A. Gade and T. Glasmacher, *Prog. Part. Nucl. Phys.* **60**, 161 (2008).
- [3] A. Obertelli, *Eur. Phys. J. Plus* **131**, 319 (2016).
- [4] D. Bazin, B. A. Brown, C. M. Campbell, J. A. Church, D. C. Dinca, J. Enders, A. Gade, T. Glasmacher, P. G. Hansen, W. F. Mueller, H. Olliver, B. C. Perry, B. M. Sherrill, J. R. Terry, and J. A. Tostevin, *Phys. Rev. Lett.* **91**, 012501 (2003).
- [5] K. Yoneda, A. Obertelli, A. Gade, D. Bazin, B. A. Brown, C. M. Campbell, J. M. Cook, P. D. Cottle, A. D. Davies, D.-C. Dinca, T. Glasmacher, P. G. Hansen, T. Hoagland, K. W. Kemper, J.-L. Lecouey, W. F. Mueller, R. R. Reynolds, B. T. Roeder, J. R. Terry, J. A. Tostevin, and H. Zwahlen, *Phys. Rev. C* **74**, 021303(R) (2006).
- [6] E. C. Simpson, J. A. Tostevin, D. Bazin, B. A. Brown, and A. Gade, *Phys. Rev. Lett.* **102**, 132502 (2009).
- [7] E. C. Simpson, J. A. Tostevin, D. Bazin, and A. Gade, *Phys. Rev. C* **79**, 064621 (2009).
- [8] D. Santiago-Gonzalez, I. Wiedenhöver, V. Abramkina, M. L. Avila, T. Baugher, D. Bazin, B. A. Brown, P. D. Cottle, A. Gade, T. Glasmacher, K. W. Kemper, S. McDaniel, A. Rojas, A. Ratkiewicz, R. Meharchand, E. C. Simpson, J. A. Tostevin, A. Volya, and D. Weisshaar, *Phys. Rev. C* **83**, 061305(R) (2011).
- [9] B. Longfellow, A. Gade, J. A. Tostevin, E. C. Simpson, B. A. Brown, A. Magilligan, D. Bazin, P. C. Bender, M. Bowry, B. Elman, E. Lunderberg, D. Rhodes, M. Spieker, D. Weisshaar, and S. J. Williams, *Phys. Rev. C* **101**, 031303(R) (2020).
- [10] A. Obertelli, A. Gade, D. Bazin, C. M. Campbell, J. M. Cook, P. D. Cottle, A. D. Davies, D.-C. Dinca, T. Glasmacher, P. G. Hansen, T. Hoagland, K. W. Kemper, J.-L. Lecouey, W. F. Mueller, R. R. Reynolds, B. T. Roeder, J. R. Terry, J. A. Tostevin, K. Yoneda, and H. Zwahlen, *Phys. Rev. C* **73**, 044605 (2006).
- [11] J. Hüfner, K. Schäfer, and B. Schürmann, *Phys. Rev. C* **12**, 1888 (1975).
- [12] W. Benenson, E. Kashy, and I. D. Proctor, *Phys. Rev. C* **8**, 210 (1973).
- [13] S. Kubono, Y. Funatsu, N. Ikeda, M. Yasue, T. Nomura, Y. Fuchi, H. Kawashima, S. Kato, H. Miyatake, H. Orihara, and T. Kajino, *Nucl. Phys. A* **537**, 153 (1992).
- [14] A. St. J. Murphy, M. Aliotta, T. Davinson, C. Ruiz, P. J. Woods, J. M. D'Auria, L. Buchmann, A. A. Chen, A. M. Laird, F. Sarazin, P. Walden, B. R. Fulton, J. E. Pearson, and B. A. Brown, *Phys. Rev. C* **73**, 034320 (2006).
- [15] C. Aa. Diget, P. Adrich, D. Bazin, M. D. Bowen, B. A. Brown, C. M. Campbell, J. M. Cook, A. Gade, T. Glasmacher, K. Hosier, S. McDaniel, D. McGlinchery, A. Obertelli, L. A. Riley, K. Siwek, J. R. Terry, J. A. Tostevin, and D. Weisshaar, *Phys. Rev. C* **77**, 064309 (2008).
- [16] P. Ruotsalainen, J. Henderson, G. Hackman, G. H. Sargsyan, K. D. Launey, A. Saxena, P. C. Srivastava, S. R. Stroberg, T. Grahm, J. Pakarinen, G. C. Ball, R. Julin, P. T. Greenlees, J. Smallcombe, C. Andreoiu, N. Bernier, M. Bowry, M. Buckner, R. Caballero-Folch, A. Chester, S. Cruz, L. J. Evitts, R. Frederick, A. B. Garnsworthy, M. Holl, A. Kurkjian, D. Kisliuk, K. G. Leach, E. McGee, J. Measures, D. Mücher, J. Park, F. Sarazin, J. K. Smith, D. Southall, K. Starosta, C. E. Svensson, K. Whitmore, M. Williams, and C. Y. Wu, *Phys. Rev. C* **99**, 051301(R) (2019).
- [17] R. Firestone, *Nucl. Data Sheets* **127**, 1 (2015).
- [18] A. Gade and B. M. Sherrill, *Phys. Scr.* **91**, 053003 (2016).
- [19] D. Morrissey, B. Sherrill, M. Steiner, A. Stolz, and I. Wiedenhoever, *Nucl. Instrum. Methods Phys. Res. B* **204**, 90 (2003).
- [20] D. Bazin, J. Caggiano, B. Sherrill, J. Yurkon, and A. Zeller, *Nucl. Instrum. Methods Phys. Res. B* **204**, 629 (2003).
- [21] J. Yurkon, D. Bazin, W. Benenson, D. Morrissey, B. Sherrill, D. Swan, and R. Swanson, *Nucl. Instrum. Methods Phys. Res. A* **422**, 291 (1999).
- [22] B. Longfellow, A. Gade, B. A. Brown, W. A. Richter, D. Bazin, P. C. Bender, M. Bowry, B. Elman, E. Lunderberg,

- D. Weisshaar, and S. J. Williams, *Phys. Rev. C* **97**, 054307 (2018).
- [23] B. Longfellow, A. Gade, B. A. Brown, D. Bazin, P. C. Bender, M. Bowry, P. D. Cottle, B. Elman, E. Lunderberg, A. Magilligan, M. Spieker, D. Weisshaar, and S. J. Williams, *Phys. Rev. C* **99**, 064330 (2019).
- [24] E. C. Simpson and J. A. Tostevin, *Phys. Rev. C* **82**, 044616 (2010).
- [25] D. Weisshaar, A. Gade, T. Glasmacher, G. Grinyer, D. Bazin, P. Adrich, T. Baugher, J. Cook, C. Diget, S. McDaniel, A. Ratkiewicz, K. Siwek, and K. Walsh, *Nucl. Instrum. Methods Phys. Res. A* **624**, 615 (2010).
- [26] B. Elman, A. Gade, D. Weisshaar, D. Barofsky, D. Bazin, P. C. Bender, M. Bowry, M. Hjorth-Jensen, K. W. Kemper, S. Lipschutz, E. Lunderberg, N. Sachmpazidi, N. Terpstra, W. B. Walters, A. Westerberg, S. J. Williams, and K. Wimmer, *Phys. Rev. C* **96**, 044332 (2017).
- [27] J. M. VonMoss, S. L. Tabor, V. Tripathi, A. Volya, B. Abromeit, P. C. Bender, D. D. Caussyn, R. Dungan, K. Kravvaris, M. P. Kuchera, R. Lubna, S. Miller, J. J. Parker, and P.-L. Tai, *Phys. Rev. C* **92**, 034301 (2015).
- [28] D. E. Alburger, C. J. Lister, J. W. Olness, and D. J. Millener, *Phys. Rev. C* **23**, 2217 (1981).
- [29] B. A. Brown and W. A. Richter, *Phys. Rev. C* **74**, 034315 (2006).
- [30] A. Gade, P. Adrich, D. Bazin, M. D. Bowen, B. A. Brown, C. M. Campbell, J. M. Cook, T. Glasmacher, P. G. Hansen, K. Hosier, S. McDaniel, D. McGlinchery, A. Obertelli, K. Siwek, L. A. Riley, J. A. Tostevin, and D. Weisshaar, *Phys. Rev. C* **77**, 044306 (2008).
- [31] W. Mueller, J. Church, T. Glasmacher, D. Gutknecht, G. Hackman, P. Hansen, Z. Hu, K. Miller, and P. Quirin, *Nucl. Instrum. Methods Phys. Res. A* **466**, 492 (2001).
- [32] S. A. Milne, M. A. Bentley, E. C. Simpson, T. Baugher, D. Bazin, J. S. Berryman, A. M. Bruce, P. J. Davies, C. A. Diget, A. Gade, T. W. Henry, H. Iwasaki, A. Lemasson, S. M. Lenzi, S. McDaniel, D. R. Napoli, A. J. Nichols, A. Ratkiewicz, L. Scruton, S. R. Stroberg, J. A. Tostevin, D. Weisshaar, K. Wimmer, and R. Winkler, *Phys. Rev. Lett.* **117**, 082502 (2016).
- [33] K. A. Chipps, R. L. Kozub, C. Sumithrarachchi, T. Ginter, T. Baumann, K. Lund, A. Lapierre, A. Villari, F. Montes, S. Jin, K. Schmidt, S. Ayoub, S. D. Pain, and D. Blankstein, *Phys. Rev. Accel. Beams* **21**, 121301 (2018).
- [34] B. Longfellow, D. Weisshaar, A. Gade, B. A. Brown, D. Bazin, K. W. Brown, B. Elman, J. Pereira, D. Rhodes, and M. Spieker, *Phys. Rev. Lett.* **125**, 232501 (2020).
- [35] O. Shehu, B. Crider, T. Ginter, C. Hoffman, T. Ogunbeku, Y. Xiao, K. Childers, P. Chowdhury, C. Fry, E. Lamere, R. Lewis, S. Liddick, B. Longfellow, S. Lyons, S. Neupane, D. Pérez-Loureiro, C. Prokop, A. Richard, U. Silwal, D. Siwakoti, D. Smith, and M. Smith, *Nucl. Instrum. Methods Phys. Res. A* **1035**, 166789 (2022).